J Sci Comput (2008) 37: 89–102
DOI 10.1007/s10915-008-9207-7

Mathematical and Numerical Aspects of a Phase-field Approach to Critical Nuclei Morphology in Solids

Lei Zhang · Long-Qing Chen · Qiang Du

Received: 5 September 2007 / Revised: 11 March 2008 / Accepted: 15 April 2008 /
Published online: 20 June 2008

Abstract We investigate a phase-field model for homogeneous nucleation and critical nucleus morphology in solids. We analyze the mathematical properties of a free energy functional that includes the long-range, anisotropic elastic interactions. We describe the numerical algorithms used to search for the saddle points of such a free energy functional based on a minimax technique and the Fourier spectral implementation. It is demonstrated that the phase-field model is mathematically well defined and is able to efficiently predict the critical nucleus morphology in elastically anisotropic solids without making *a priori* assumptions.

Keywords Nucleation · Critical nuclei · Phase field simulation · Anisotropic elasticity · Solid state phase transformation

1 Introduction

Nucleation refers to a process that takes place when a material becomes metastable with respect to its transformation to a new state (solid, liquid, and gas) or new crystal structure. It is perhaps the most common physical phenomenon in nature. Predicting nucleation rate and its dependence on composition/temperature is critical for controlling the microstructure of a material and thus its properties.

L. Zhang
Department of Mathematics, Penn State University, PA 16802, Centre County, USA
e-mail: zhang_l@math.psu.edu

L.-Q. Chen
Department of Materials Science and Engineering, Penn State University, PA 16802, Centre County, USA
e-mail: lqc3@psu.edu

Q. Du (✉)
Department of Mathematics and Department of Materials Science and Engineering, Penn State University, PA 16802, Centre County, USA
e-mail: qdu@math.psu.edu

Recently, we proposed a phase-field model for predicting the nucleus morphology in solids in the presence of interfacial energy anisotropy and anisotropic elastic interactions [40]. Phase-field methods have been extensively applied to model microstructure evolution for various materials processes including solidification, solid state phase transformations, grain or phase coarsening, etc. [5]. They have also been used in fluid mechanics, biomechanics and other settings [1, 9]. The diffuse interface (phase field) approach is an attractive and popular tool in materials science simulation and design since the evolution of different microstructural features can be predicted by means of a single set of equations, and there are no explicit boundary conditions specified at interfaces.

In this paper, we study the mathematical formulation of the diffuse-interface description of a critical nucleus and the numerical algorithms obtaining the critical order parameter profiles. In particular, we discuss the existence of saddle points, the minimax algorithm, and the Fourier spectral approximations. We also present numerical examples in both two and three dimensional spaces to illustrate the effectiveness of this computational modeling approach.

2 Background

The classical nucleation theory was first developed in 1930s. It is still the most often used theory in studying nucleation as of today. The earlier studies mostly considered phase changes in fluids such as a liquid droplet in a vapor phase. It was then natural to adopt spherical shapes for the critical nuclei. The thermodynamic properties of a nucleus are assumed to be the same as in the corresponding bulk phase. The calculation of a critical spherical droplet in a supersaturated exterior phase is then performed, with the size of a critical nucleus being determined as a result of competition between the bulk free energy reduction and interfacial energy increase. For instance, the free energy change accompanying the formation of a new particle can be given by

$$\Delta G = V\Delta g + A \cdot \gamma \tag{1}$$

where V is volume of particle, A is surface area, Δg is chemical free energy change per unit volume, γ is the specific interfacial energy. For a spherical particle of radius r,

$$\Delta G = \frac{4}{3}\pi r^3 \Delta g + 4\pi r^2 \gamma. \tag{2}$$

The radius r^* of the critical nucleus must then be such that

$$r^* = -\frac{2\gamma}{\Delta g}.$$

The critical free energy of formation of a critical nucleus is given by

$$\Delta G^* = \frac{16\pi\gamma^3}{3(\Delta g)^2}. \tag{3}$$

The classical theories have been utilized to interpret kinetics of many phase transformations involving solids including solid to solid transformations, and have had some success for providing good descriptions on the nucleation kinetics for some systems, despite the assumption on the spherical critical nuclei shapes. On the other hand, nucleation in solids is generally significantly more complicated than that in fluids. This can be understood from

several aspects: first of all, due to the crystallographic nature of most solids, the interfacial energy between a nucleus and the matrix is generally anisotropic, which thus leads to non-spherical minimum surface shapes; meanwhile, there are typically mismatches between the lattice parameters of a new phase and the corresponding parent, so an elastic energy is generated during the nucleation to accommodate such lattice mismatch between a nucleus and the matrix. Since the elastic energy contribution depends on the morphology of a nucleus and lattice mismatch between the nucleus and the matrix, a direct geometric construction of the shape of a critical nucleus is thus very difficult. It is particularly challenging in cases where both elastic energy and surface energy anisotropy exist.

When applying the classical nucleation theory to solid state transformations, the shape of a nucleus is often given *a priori* [2], the elastic energy contribution to nucleation is incorporated as an extra nucleation barrier, i.e., the size of a nucleus is scaled by a factor related to $\Delta f_v + E_e$, where Δf_v is the bulk driving force for nucleation and E_e is the elastic strain energy contribution.

3 Diffuse Interface Model

The non-classical theory was pioneered by Cahn and Hilliard [4]. For subsequent studies, generalization and application to nucleation in solids, we refer to the discussion in the works of [6, 17, 20, 33, 35, 38]. It is mentioned in [20] that sharp-interface treatments are sometimes less effective than diffuse interface theories in comparing with experiment. It should be pointed out that these existing diffuse interface theories for nucleation in solids have largely ignored the anisotropic interfacial energy and anisotropic long-range elastic interactions until recently [40].

We now describe the phase field diffuse-interface model considered in [40]. First, as an illustration, only a structural transition is assumed with no compositional changes. We also assume that the structural difference between the parent phase and the nucleating phase can be sufficiently described by a single order parameter η. Extensions to more general cases can also be considered in a similar fashion and will be pursued in the future.

At a given temperature, the free energy dependence on η is described by a double-well potential

$$f(\eta) = \frac{1}{4} - \frac{\eta^2}{2} + \frac{\eta^4}{4} - \lambda h(\eta)$$

with local energy wells at $\eta = \pm 1$ respectively and $h(\eta) = (3\eta - \eta^3)/2$ so that 2λ determines the well depth difference which gives the bulk free energy driving force for the phase transformation from the $\eta = -1$ state to the $\eta = 1$ state. In Fig. 1, f is plotted for two values of λ.

The total free energy of an inhomogeneous system described by a spatial distribution of η is given by:

$$E = \int_\Omega \left(f(\eta) + \frac{1}{2} |M \nabla \eta|^2 \right) d\mathbf{x}.$$

Here, the domain $\Omega = (-1, 1)^d$ is used with d being the space dimension and a periodic boundary condition is used for the order parameter η. The period is taken to be large in comparison to the size of the nucleus to avoid any possible boundary effect. M is the gradient energy coefficient which is a constant diagonal tensor in Ω for isotropic interfacial energy. For anisotropic interfacial energy, M may be made either directionally dependent or

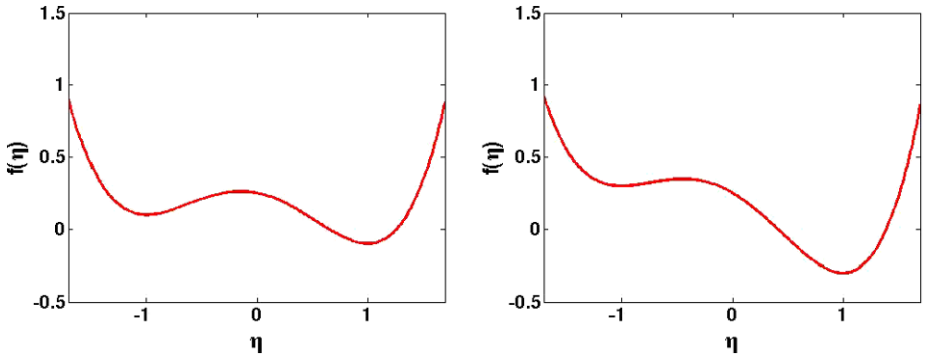

Fig. 1 Double well potentials with driving forces $\lambda = 0.1, 0.3$

dependent on the derivatives of η. To incorporate the effect of long-range elastic interactions on the morphology of a critical nucleus, and thus the nucleation barrier, the computation of the elastic energy E_e is needed. Assuming that the elastic modulus is anisotropic but homogeneous, the microscopic elasticity theory of Khachaturyan [26] is often used in phase field simulations. For example, the elasticity effect is incorporated by expressing the elastic strain energy as a function of field variables (see the discussion in, for example, [23, 28, 32, 36, 39], and an earlier work [12]). To be specific, the total energy is given by

$$E_t = \int_\Omega \left(f(\eta) + \frac{1}{2}|M\nabla\eta|^2 \right) d\mathbf{x} + E_e \tag{4}$$

where E_e is the elastic energy defined as

$$E_e = \int_\Omega e d\mathbf{x}; \tag{5}$$

with the elastic energy density e calculated from:

$$e = \frac{1}{2} C_{ijkl} \varepsilon_{ij}^{el} \varepsilon_{kl}^{el}.$$

The summation convention is used here. For a cubic material with its three independent elastic constants c_{11}, c_{12} and c_{44} in the Voigt's notation, the elastic energy density takes on the form [26]:

$$\begin{aligned} e = {} & \frac{1}{2} c_{11}((\varepsilon_{11}^{el})^2 + (\varepsilon_{22}^{el})^2 + (\varepsilon_{33}^{el})^2) + c_{12}(\varepsilon_{11}^{el}\varepsilon_{22}^{el} + \varepsilon_{11}^{el}\varepsilon_{33}^{el} + \varepsilon_{22}^{el}\varepsilon_{33}^{el}) \\ & + 2c_{44}((\varepsilon_{12}^{el})^2 + (\varepsilon_{13}^{el})^2 + (\varepsilon_{23}^{el})^2). \end{aligned}$$

Here the elastic strain ε^{el} is the difference between the total strain ε and stress-free strain ε^* since stress-free strain does not contribute to the total elastic energy, i.e.

$$\varepsilon_{ij}^{el} = \varepsilon_{ij} - \varepsilon_{ij}^*,$$

where the stress-free strain is

$$\varepsilon_{ij}^* = (\varepsilon_0)_{ij}(\eta - \eta_0).$$

Here, $(\varepsilon_0)_{ij}$ is a constant tensor and η_0 is the average order parameter value. The total strain ε_{ij} may be represented as the sum of homogeneous and heterogeneous strains:

$$\varepsilon_{ij} = \bar{\varepsilon}_{ij} + \delta\varepsilon_{ij}.$$

The homogeneous strain is defined in such a way so that

$$\int_\Omega \delta\varepsilon_{ij} d\mathbf{x} = 0.$$

The heterogeneous strain is related to the local displacement field $\{v_k\}$ by the usual elasticity relation,

$$\delta\varepsilon_{ij} = \frac{1}{2}\left(\frac{\partial v_i}{\partial x_j} + \frac{\partial v_j}{\partial x_i}\right).$$

In the mechanical equilibrium, it satisfies the elasticity equation

$$\frac{\partial \sigma_{ij}}{\partial x_j} = 0$$

with the stress components $\sigma_{ij} = c_{ijkl} e_{kl}$.

The elasticity equation with periodic boundary conditions can be solved in the Fourier space which leads to a more explicit form of E_e. Through detailed derivations, it is shown in [26] that, for the case of a simply connected coherent inclusion in an anisotropic solid with cubic symmetry, if the phase transformation involves only one type of crystal lattice, the elasticity energy contribution can be further simplified to

$$E_e = \frac{1}{2(2\pi)^d} \int_{\hat{\Omega}} d\mathbf{k} B(\mathbf{n}) |\hat{\eta}(\mathbf{k}) - \hat{\eta}_0(\mathbf{k})|^2. \tag{6}$$

Here, $\hat{\eta}(\mathbf{k})$ and $\hat{\eta}_0(\mathbf{k})$ are the Fourier transform of $\eta(\mathbf{x})$ and η_0 respectively. The integration in (6) is over the reciprocal space $\hat{\Omega}$ of the reciprocal lattice vector $\mathbf{k}$, $\mathbf{n} = \mathbf{k}/|\mathbf{k}| = (n_1, n_2, n_3)$ is the normalized unit vector and in three dimensions, and the term $B(\mathbf{n})$ is given by

$$\begin{aligned} B(\mathbf{n}) &= 3(c_{11} + 2c_{12})\epsilon_0^2 \\ &\quad - \frac{(c_{11} + 2c_{12})^2 \epsilon_0^2 (1 + 2\zeta s(\mathbf{n}) + 3\zeta^2 n_1^2 n_2^2 n_3^2)}{c_{11} + \zeta(c_{11} + c_{12}) s(\mathbf{n}) + \zeta^2 (c_{11} + 2c_{12} + c_{44}) n_1^2 n_2^2 n_3^2} \end{aligned} \tag{7}$$

where we employ the Voigt's notation, and for the cubic materials, we let $\zeta = (c_{11} - c_{12} - 2c_{44})/c_{44}$ be the elastic anisotropic factor, $(\varepsilon_0)_{ij} = \epsilon_0 \delta_{ij}$ with ϵ_0 being the lattice mismatch between the nucleating new cubic phase and the parent cubic phase, and $s(\mathbf{n}) = n_1^2 n_2^2 + n_1^2 n_3^2 + n_2^2 n_3^2$. We set in particular that $\mathbf{n} = 0$ if $\mathbf{k} = 0$.

Taking into account the long-range elastic interactions and surface energy anisotropy, the increase in the total free energy arising from the order parameter fluctuation in an initially homogeneous state with η_0 is given by

$$\Delta E_{total}(\eta) = \int_\Omega \left(\delta f(\eta) + \frac{\alpha_x}{2}\eta_x^2 + \frac{\alpha_y}{2}\eta_y^2\right) d\mathbf{x} + \beta E_e \tag{8}$$

where $\delta f(\eta) = f(\eta) - f(\eta_0)$ and E_e is given by (6). Rather than varying the magnitudes of lattice mismatch and elastic constants, a factor β is introduced to study the effect of relative elastic energy contribution to chemical driving force on the critical nucleus morphology.

4 Saddle Points

Since nucleation takes place by overcoming the minimum energy barrier, a critical nucleus is defined as the spatial order parameter fluctuation which has the minimum free energy increase among all fluctuations which lead to nucleation. Therefore, we may find the critical nucleus by computing the saddle points of the energy functional of the order parameter η, that has the highest energy in the minimum action path which is the path whose highest energy is the lowest among all possible paths. This is consistent with the large derivation theory which states that the most probable path (that minimizes the action [27]) passes through the saddle point in the large time limit.

Let us first study some basic theories concerning the existence of saddle points. For simplicity, we consider the case of isotropic surface energy only, that is, we take $\alpha_x = \alpha_y$. In this case, for the convenience of mathematical analysis, a different scaling is often introduced so that it is equivalent to consider the saddle points of the following functional:

$$E_\epsilon(\eta) = \int_\Omega \left[\frac{\epsilon}{2}|\nabla\eta|^2 + \frac{1}{4\epsilon}(\eta^2-1)^2 + \frac{\lambda}{2}(3\eta-\eta^3) \right] d\mathbf{x} + \frac{\beta}{2(2\pi)^d} \int_{\hat{\Omega}} d\mathbf{k} B(\mathbf{n}) |\hat{\eta}(\mathbf{k}) - \hat{\eta}_0(\mathbf{k})|^2, \tag{9}$$

with $B(\mathbf{n})$ as given by (7). To be more precise, we consider the variation of the energy E_ϵ in the Hilbert space $H_p^1(\Omega)$ which is the standard H^1 Sobolev space of the periodic functions defined on Ω.

For the parameter range of interest to us, we may assume that there are two positive constants M_1 and M_2 such that

$$0 \le M_1 \le B(\mathbf{n}) \le 3(c_{11}+2c_{12})\epsilon_0^2 = M_2$$

uniformly in the unit sphere.

In the literature, a popular approach to study the existence of saddle points within the framework of calculus of variation is given by the mountain pass theorem, which often relies on the so called *minimax* technique [34]. Another approach has been developed recently in [25] to relate a saddle point of E_ϵ with its Γ-limit functional. In all these works, a key condition for the applicability is the Palais-Smale compactness condition:

Definition 1 (PS condition) Given a Hilbert space H, and a C^1 functional $E : H \to R$, a sequence $\{u_k\}_1^\infty$ in H is said to be a Palais-Smale sequence if

$$\lim_{k\to\infty} \|\delta E(u_k)\|_{H^{-1}} = 0 \quad \text{and} \quad \{E(u_k)\}_1^\infty \text{ is bounded.} \tag{10}$$

The functional F is said to satisfy the Palais-Smale condition if every Palais-Smale sequence is precompact in H.

Here H^{-1} refers to the conventional dual space of H [13] and δE denotes the first variation of the energy E. We now state the result that verifies the PS condition for the functional E_ϵ given by (9).

Theorem 1 *The functional $E_\epsilon = E_\epsilon(\eta)$ given by (9) satisfies the Palais-Smale condition in $H_p^1(\Omega)$.*

Proof We follow similar lines as in [25]. Suppose that $\{\eta_k\}$ is a sequence satisfying the conditions

$$\sup_k E_\epsilon(\eta_k) < \infty, \qquad \lim_{k\to 0} \|\delta E_\epsilon(\eta_k)\|_{H^{-1}} = 0.$$

Here, in the weak sense, the first energy variation is given by

$$\delta E_\epsilon(\eta) = -\epsilon\Delta\eta + \frac{1}{\epsilon}(\eta^3 - \eta) + \frac{3\lambda}{2}(\eta^2 - 1) + \frac{\beta}{(2\pi)^d}\int_{\hat{\Omega}} B(\mathbf{n})(\hat{\eta}(\mathbf{k}) - \hat{\eta}_0(\mathbf{k}))e^{i\mathbf{kx}}d\mathbf{k}.$$

By the energy bound, we get a uniform H^1 bound. Hence, there is a subsequence $\{k_j\}$ such that

$$\eta_{k_j} \rightharpoonup \eta \quad \text{in } H_p^1(\Omega) \quad \text{and} \quad \eta_{k_j} \to \eta \quad \text{in } L^p(\Omega), \quad 1 \le p < 2d/(d-2)$$

for some $\eta \in H_p^1(\Omega)$. By the assumption on $B(\mathbf{n})$ and the Parseval identity, we easily see that

$$\lim_{j\to\infty}\int_{\hat{\Omega}} d\mathbf{k}B(\mathbf{n})|\hat{\eta}_{k_j}(\mathbf{k}) - \hat{\eta}_0(\mathbf{k})|^2 = \int_{\hat{\Omega}} d\mathbf{k}B(\mathbf{n})|\hat{\eta}(\mathbf{k}) - \hat{\eta}_0(\mathbf{k})|^2.$$

By the conditions

$$\langle \delta E_\epsilon(\eta_k), \eta_k\rangle \to 0 \quad \text{and} \quad \langle \delta E_\epsilon(\eta_k), \eta\rangle \to 0,$$

we then get

$$\begin{aligned}\lim_{j\to\infty}\int_\Omega |\nabla\eta_{k_j}|^2 d\Omega &= \lim_{j\to\infty}\left\{\int_\Omega g(\eta_{k_j})d\Omega - \frac{\beta}{\epsilon(2\pi)^d}\int_{\hat{\Omega}} d\mathbf{k}B(\mathbf{n})|\hat{\eta}_{k_j}(\mathbf{k}) - \hat{\eta}_0(\mathbf{k})|^2\right\}\\ &= \int_\Omega g(\eta)d\Omega - \frac{\beta}{\epsilon(2\pi)^d}\int_{\hat{\Omega}} d\mathbf{k}B(\mathbf{n})|\hat{\eta}(\mathbf{k}) - \hat{\eta}_0(\mathbf{k})|^2\\ &= \int_\Omega |\nabla\eta|^2 d\Omega\end{aligned}$$

where $g = g(\eta)$ denotes

$$g(\eta) = \frac{1}{\epsilon^2}(\eta^4 - \eta^2) + \frac{3\lambda}{2\epsilon}(\eta^3 - \eta).$$

The norm convergence with the weak convergence together means that the sequence is convergent strongly in H^1, we thus have the PS condition satisfied. □

With the PS condition, one may apply the mountain pass type theorems to get the saddle point of the energy [34]. For a given constant positive driving force, it can be seen that when ϵ is suitably small, on the boundary of a small H^1 ball of the solution $\eta_0 = -1$, the energy is strictly larger than $E_\epsilon(\eta_0)$, moreover, for small ϵ, E_ϵ at $\eta = 1$ is strictly less than the energy $E_\epsilon(\eta_0)$. The mountain pass theorem can thus be applied [34] and there must be a saddle connecting the path between $\eta = \eta_0 = -1$ and $\eta = 1$ with the lowest energy barrier. Due to the periodic boundary condition, it is possible to have a constant solution as the saddle point. For small ϵ, the energy of such a trivial saddle is of $O(\epsilon^{-1})$, but one may easily construct a path (for instance via tanh profiles [9]) which would have an energy barrier of $O(1)$. Thus, a non-trial saddle point exists.

With the PS condition, one may also adopt similar techniques as that presented in [25] to connect the saddle point of E_ϵ with the saddle point of the Γ-limit as $\epsilon \to 0$. Let us briefly recall the concept of Γ-convergence which is defined through two requirements: given a Banach space U, a sequence of functionals, $E_\epsilon : U \to R$, Γ-converges to a limiting functional E_0 as $\epsilon \to 0$ if for every $u \in U$ one has

(i) whenever $\{u_\epsilon\} \subset U$ converges to u, $\liminf_{\epsilon\to 0} E_\epsilon(u_\epsilon) \geq E_0(u)$, and
(ii) there exists a sequence $\{\tilde{u}_\epsilon\} \subset U$ such that $\tilde{u}_\epsilon$ converges to u and $\lim_{\epsilon\to 0} E_\epsilon(\tilde{u}_\epsilon) = E_0(u)$.

The notion of Γ-convergence has proven to be a powerful tool to study the limit of minimizers of functional sequences $E_\epsilon : U \to R$ whose conventional limit is typically defined on another Banach space V which has a weaker topology. For example, in [18], the Γ-convergence of the minimizers for a free energy of the form (4), which includes both the interfacial energy and the elastic misfit energy as that given in (5), has been studied. More recently, Γ-convergence was also used to study the unstable saddle points of Ginzburg-Landau like functionals in [25]. The latter naturally applies to the case we consider here. The limiting functional is given as follows: for any $v \in L^1(\Omega)$,

$$E_0(v) = \begin{cases} \frac{\sqrt{2}}{3}\int_\Omega |\nabla v| d\Omega + \int_\Omega \lambda v d\Omega \\ \quad + \frac{\beta}{2(2\pi)^d}\int_{\hat{\Omega}} d\mathbf{k} B(\mathbf{n})|\hat{v}(\mathbf{k}) - \hat{\eta}_0(\mathbf{k})|^2, & \text{if } v \in BV(\Omega, \{\pm 1\}), \\ \infty, & \text{otherwise.} \end{cases}$$

If the zero level set of v is rectifiable, then by the co-area formula, we may also use the perimeter of the zero level set of v to replace the first integral in the functional. The second term is obviously the bulk energy (volume) difference, and the third term is due to the elastic contribution. We thus have the problem of finding the critical point of the functional E_0 as the Γ-limit. This is also commonly referred as the sharp interface limit of the phase field model. Note that the form given here does not require the explicit use of the displacement field and is simpler than the case considered in [18, 19].

The saddle point of E_0 can also be computed via direct geometric modeling of the zero level set of v, especially when a simply connected inclusion is of interest. A level set approach can also be developed similar to the case without the elastic energy. We however elect to work with the original phase field energy, both for its rich physical origin and for future coupling with the phase field simulation of the microstructure evolution [5]. The sharp interface analysis is only given here to provide some theoretical understanding.

5 Numerical Algorithm

The saddle points to be computed are the solutions of the Euler-Lagrange equation of ΔE_{total}, or without loss of generality, that of E_ϵ:

$$\epsilon\Delta\eta = \frac{\eta^3 - \eta}{\epsilon} + \lambda(\eta^2 - 1) + \frac{\beta}{(2\pi)^d}\int_{\hat{\Omega}} B(\mathbf{n})(\hat{\eta}(\mathbf{k}) - \hat{\eta}_0(\mathbf{k}))e^{i\mathbf{kx}} d\mathbf{k}, \tag{11}$$

in the domain Ω, subject to the periodic boundary condition.

The above equation can be viewed as a nonlocal perturbation to some well studied semilinear elliptic equation. Due to the periodic boundary condition, the non-locality can be efficiently treated in the Fourier space, thus a Fourier spectral approximation is appropriate.

For analysis of Fourier spectral approximations, we borrow the abstract framework developed in [3]. Taking for instance β as a parameter, we may view the computed Fourier spectral solution as an approximation to an nonsingular branch of solutions of (11). We denote $\eta_N(\beta)$ as the spectral solution with N Fourier modes in each variable directions. With given ϵ, the phase field solutions are smooth (and analytic), and the nonlinear part as well as the part involving the elastic contributions can be seen as a smooth compact perturbation to the principal linear elliptic part, moreover, it is easy to see that except at certain critical values of β, each solution branch is smooth in β and is isolated. We then have a general error estimates for the Fourier spectral approximation:

Theorem 2 *Let Λ be a compact interval in R, and let $\eta = \eta(\beta)$ be a regular smooth solution branch of (11). Then, for N sufficiently large, there exists a unique regular branch of $\eta_N = \eta_N(\beta)$ in a neighborhood of $\eta = \eta(\beta)$ which is the approximate Fourier spectral solution of (11) such that*

$$\lim_{N\to\infty} \|\eta(\beta) - \eta_N(\beta)\|_{H^1_p(\Omega)} = 0.$$

Moreover, there exist positive constants c and σ, independent of N for N large, such that

$$\|\eta(\beta) - \eta_N(\beta)\|_{H^1_p(\Omega)} \le ce^{-\sigma N}. \tag{12}$$

The proof of the above theorem can be constructed by coupling standard error estimates for the linear elliptic equations with the general theory for nonlinear problems developed in [3] (for applications to Ginzburg-Landau and phase field type of models that are similar to ones considered here, one may also consult [8, 10]). We omit the details. The numerical results reported later confirm such accuracy. Naturally, in many practical situations, one may be interested in the dependence of the numerical accuracy with the model parameters such as the interfacial width parameter ϵ. We refer to [15] for some studies on more precise estimates with respect to the parameters. Computationally, it is found that the spectral scheme performs well, even for very small ϵ, in comparing with low order finite difference or finite element schemes, but a complete theoretical understanding is lacking at the moment. We note that an adaptive spectral scheme has also been introduced recently [14] which can be even more effective in resolving the thin interfacial domain.

In the numerical implementation, we do not solve the Euler-Lagrange equation directly as the saddle points are unstable critical points of the energy. Instead, more sophisticated numerical schemes are used to assure robustness and stability. There are various approaches for the numerical solution of variational problems. While the most notable ones are for finding minimizers, algorithms have also been developed to find minimum energy paths and to search for saddle points [11, 16, 21, 22, 24, 30]. Here, we employ an algorithm which adopts the *minimax* technique in the calculus of variation and optimization [31, 34] to find the saddle points. A natural idea of the minimax algorithm is to first define a solution submanifold $\mathcal{M}$ such that a local minimum point of ΔE_{total} on $\mathcal{M}$ yields a saddle point on the full manifold. Thus the problem becomes a minimization of ΔE_{total} on the submanifold, and a saddle point becomes stable on the submanifold $\mathcal{M}$. Here, to ensure stability and monotonicity, a steepest descent search is applied to approximate a local minimizer of ΔE_{total} on submanifold $\mathcal{M}$. Meanwhile, it is imperative that a *return rule* is used to prevent the descent search from leaving the submanifold so as to guarantee the convergence of the algorithm.

We follow the approach studied in [30] which is outlined below:

1. For $k = 0$, take a direction ν_0 at a local minimum η_0, define

$$\mathcal{M}_0 = \{\eta_0 + \text{span}\{\nu_0\}\}$$

and search for a local maximum in $\mathcal{M}_0$, i.e., solve

$$w^k = p(\nu_0) := \arg\max_{u \in \mathcal{M}_0} \Delta E_{total}(u).$$

2. For $k \geq 0$, compute the variational gradient g^k of ΔE_{total} at w^k. If $\|g^k\|$ is less than some tolerance, stop and output w^k as a critical nucleus, else goto Step 3.
Given a step-size parameter $\hat{b}_k$, let

$$\mathcal{M}_b^{k+1} = \{\nu_k + \text{span}\{\nu_b^k\}\}$$

with ν_b^k being the unit vector in the direction of $\nu^k - bg^k$ and b in $(0, \hat{b}_k)$, let

$$p(\nu_b^k) := \arg\max_{u \in \mathcal{M}_b^{k+1}} \Delta E_{total}(u).$$

Solve

$$b^* := \arg\min_{0<b<\hat{b}_k} \Delta E_{total}(p(\nu_b^k)),$$

set $\nu^{k+1} = \nu_{b^*}^k$, $w^{k+1}=p(\nu^{k+1})$, update k by $k + 1$ and go to Step 2.

Here arg max and arg min denote respectively the variables at which the maximum and minimum are attained. We refer to [30] for additional discussions and the convergence properties of the above algorithm.

For computational efficiency, we find that it works well to choose a tanh profile as the initial search direction in the first step. The argument of the tanh function is a scaled distance to some prescribed level set. In Step 2, the number $\hat{b}_k$ is used to control the step-size of the steepest descent search. This is important for the stability of the algorithm. Again, in each of the steps, the Fourier spectral methods are used to solve the resulting PDEs or to compute the energy variations, which allows very efficient computation via FFT. In addition, we note that an inner product given by the integral of the product of the functions and their gradients is adopted in Step 2 to define the variational gradient g^k which is computed again via FFT in the Fourier spectral discretization. This technique is similar to the use of a spectrally equivalent preconditioner for the Hessian matrix in the numerical solution of minimization problems.

6 Numerical Examples

We now present illustrative numerical examples that demonstrate the convergence of the numerical scheme and examples that offer some hints on the critical nucleus morphologies in cubically anisotropic systems. We take the energy scaled in the form (9) with $\eta_0 = -1$, $c_{11} = 250$, $c_{12} = 150$, $c_{44} = 100$ in all of our simulations. The other parameters may change for different cases and they are specified later.

First, we conduct a series of numerical experiments in two dimensions to verify the spectral accuracy of the computed solution. Since for most of the physically relevant cases, there

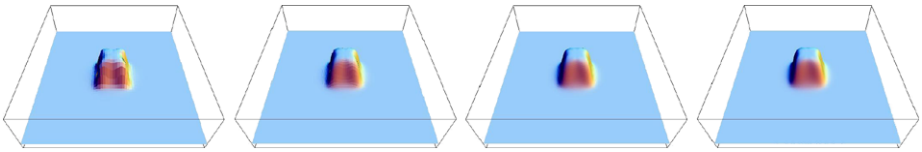

Fig. 2 Plots of critical nuclei for $\epsilon = 1/32$

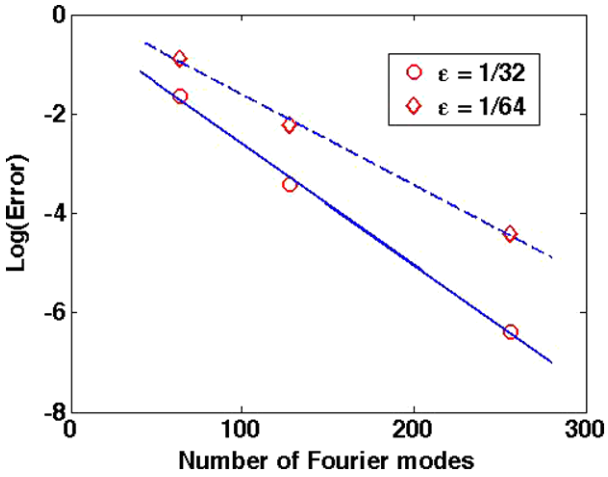

Fig. 3 Logarithms of the H^1 errors for $\epsilon = 1/32$ and $1/64$

Table 1 Errors of Fourier spectral solutions for fixed and changing ϵ

Fourier modes	$\epsilon = 1/32$	$\epsilon = 1/64$	$\epsilon = 2/N$
$N = 64$	0.1926	0.4134	1.0509e−002
$N = 128$	0.0326	0.1075	2.8876e−003
$N = 256$	0.0017	0.0121	5.3744e−004

is no exact analytic solution available, we simply compare other numerical solutions with that computed with the most number of Fourier modes (with the highest level of numerical resolution). The comparison is done in two fronts, one with a fixed interfacial width $\epsilon = 1/32$, while the number of Fourier modes changes from 64^2 to 128^2, 256^2 and finally 512^2. Here, we take $\lambda = 6$ and $\beta = 0.3$ and $\epsilon_0 = 0.1$.

The plots of the computed solutions are given respectively in Fig. 2 for $\epsilon = 1/32$, corresponding to different grids. The non-convex shape of the critical nuclei is a signature property due to the anisotropic elastic energy contribution [40].

We show in Table 1 the differences of the solutions with that on the 512^2 grid, the errors in the H^1 norm are given for the cases of $\epsilon = 1/32$ and $\epsilon = 1/64$ respectively. To better examine the convergence rate as $N \to \infty$ for a given ϵ, in Fig. 3, the logarithms of the H^1 error norms given in Table 1 are plotted with respect N, as stars and circles respectively corresponding to the different values of ϵ. The solid and dash lines are the respective best least square fits of the data points using linear polynomials. The linear behavior in the logarithm of the error provides a clear illustration of the spectral accuracy of the numerical solutions.

We also compute the solutions with a gradually decreasing ϵ with increasing number of Fourier modes. Specifically, we take $\epsilon = 2/N$ where N is the number of Fourier modes used

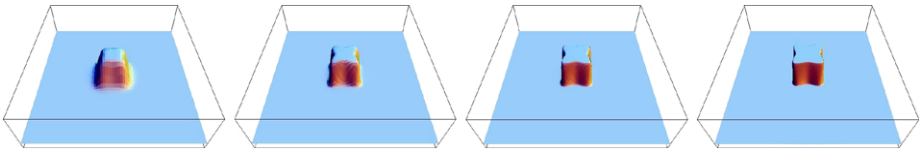

Fig. 4 Plots of critical nuclei for $\epsilon = 2/N$ with $N = 64, 128, 256, 512$

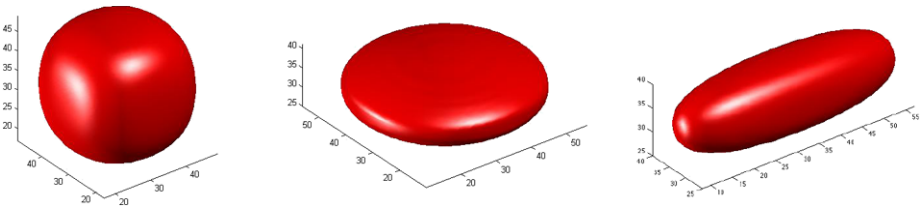

Fig. 5 3D critical nuclei for $\beta = 0.2$ (*left*), 0.4 (*center*) and 0.5 (*right*)

in each direction. The plots of the computed solutions are given in Fig. 4. We have found that adequate resolutions are maintained for all values of ϵ, and, as expected, the interfacial layers are getting sharper for smaller ϵ while the shapes remain nearly identical. Since in the sharp interface limit, the solution is no longer in H^1, we measure the L^2 difference in the norms instead, and the results are given as errors in Table 1 also (the right-most column), which illustrate the convergence of the solutions in such a limit. It remains as a challenge, however, to quantify the optimal rate of convergence as $N \to \infty$ when ϵ is taken to be dependent of N [15].

Next, we present some three dimensional results to show the effect of different elastic energy contributions in Fig. 5. Here, we take $\lambda = 5$ and $\epsilon_0 = 0.1$. It can be seen that the long-range elastic interactions can dramatically change the critical nucleus morphology. A strong elastic interaction may lead to critical nuclei with cuboidal, plate-like, needle-like, or even non-convex shapes. We refer to similar findings and further discussions given in [40] for the two dimensional case and more detailed analysis in three dimension [41].

7 Conclusion

Our recent works demonstrate that the morphology of a critical nucleus, or a critical fluctuation in elastically anisotropic solids can be predicted by a combination of the diffuse-interface approach and the minimax algorithm. The nucleation profile calculation is shown to be mathematically well-posed with the diffuse-interface energy under consideration. Its relation to sharp interface models is also revealed. Although there have been extensive theoretical studies of particle morphologies during growth or coarsening by minimizing the total interfacial and elastic strain energy [7, 19, 29, 37], our method provides a new approach to predict the morphologies of saddle-point critical nuclei without any *a priori* assumptions on the shapes. The Fourier spectral discretization works efficiently in the implementation of the minimax algorithm and provides an efficient and robust procedure for the critical nuclei calculation. Our calculations reveal the fascinating possibility of nuclei with non-convex shapes and the formation of critical nuclei whose symmetry is lower than both the new phase and the original parent matrix. It should be noted that the present work ignores the possible

presence of defects such as dislocations and interfaces, i.e. heterogeneous nucleation. We are presently studying generalizations to such cases as well as the effective coupling of the critical profile calculation with the phase field simulation of microstructure evolutions.

Acknowledgement This work is supported in part by NSF-DMR ITR 0205232, NSF-DMS 0712744 and by NSF-IIP 541674 Center for Computational Materials Design (CCMD). The authors would like to thank the referees for their valuable suggestions.

References

1. Anderson, D., McFadden, G., Wheeler, A.: Diffuse-interface methods in fluid mechanics. Annu. Rev. Fluid Mech. **30**, 139–165 (1998)
2. Brener, E., Iordanskii, S., Marchenko, V.: Elastic effects on the kinetics of a phase transition. Phys. Rev. Lett. **82**, 1506–1509 (1999)
3. Brezzi, F., Rappaz, J., Raviart, P.: Finite dimensional approximation of nonlinear problems part I: branches of nonsingular solutions. Numer. Math. **36**, 1–25 (1980)
4. Cahn, J., Hilliard, J.: Free energy of a nonuniform system, III. Nucleation in a two-component incompressible fluid. J. Chem. Phys. **31**, 688–699 (1959)
5. Chen, L.Q.: Phase-field models for microstructure evolution. Annu. Rev. Mater. Sci. **32**, 113–140 (2002)
6. Chu, Y., Moran, B., Reid, A., Olson, G.: A model for nonclassical nucleation of solid-solid structural phase transformations. Metall. Mater. Trans. A **31**, 1321–1331 (2000)
7. Conti, S., Schweizer, B.: A sharp-interface limit for a two-well problem in geometrically linear elasticity. Arch. Ration Mech. Anal. **179**, 413–452 (2006)
8. Du, Q., Gunzburger, M., Peterson, J.: Analysis and approximation of the Ginzburg-Landau Model of superconductivity. SIAM Rev. **34**, 54–81 (1992)
9. Du, Q., Liu, C., Wang, X.: A phase field approach in the numerical study of the elastic bending energy for vesicle membranes. J. Comput. Phys. **198**, 450–468 (2004)
10. Du, Q., Zhu, L.: Analysis of a mixed finite element method for a phase field elastic bending energy model of vesicle membrane deformation. J. Comput. Math. **24**, 265–280 (2006)
11. E, W., Ren, W., Vanden-Eijnden, E.: String method for the study of rare events. Phys. Rev. B **66**, 052301 (2002)
12. Eshelby, J.: The elastic field outside an ellipsoidal inclusion. Proc. R. Soc. Lond. A **252**, 561–569 (1959)
13. Evans, L.C.: Partial Differential Equations. Am. Math. Soc., Providence (1998)
14. Feng, W., Yu, P., Hu, S., Liu, Z., Du, Q., Chen, L.: Spectral implementation of an adaptive moving mesh method for phase-field equations. J. Comput. Phys. **220**, 498–510 (2006)
15. Feng, X., Prohl, A.: Analysis of a fully discrete finite element method for the phase field model and approximation of its sharp interface limits. Math. Comput. **73**, 541–567 (2004)
16. Fischer, S., Karplus, M.: Conjugate peak refinement: an algorithm for finding reaction paths and accurate transition states in systems with many degrees of freedom. Chem. Phys. Lett. **194**, 252–261 (1992)
17. Gagne, C., Gould, H., Klein, W., Lookman, T., Saxena, A.: Simulations of spinodal nucleation in systems with elastic interactions. Phys. Rev. Lett. **95**, 095701 (2005)
18. Garcke, H., Kwak, D.: On asymptotic limits of Cahn-Hilliard systems with elastic misfit. In: Analysis, Modeling and Simulation of Multiscale Problems, pp. 87–111. Springer, Berlin (2006)
19. Garcke, H., Rumpf, M., Weikard, U.: The Cahn-Hilliard equation with elasticity, finite element approximation and qualitative analysis. Interfaces Free Bound. **3**, 101–118 (2001)
20. Gránásy, L.: Diffuse interface theory of nucleation. J. Non-Cryst. Solids **162**, 301–303 (1993)
21. Henkelman, G., Jonsson, H.: A dimer method for finding saddle points on high dimensional potential surfaces using only first derivatives. J. Chem. Phys. **111**, 7010–7022 (1999)
22. Henkelman, G., Uberuaga, B., Jonsson, H.: A climbing image nudged elastic band method for finding saddle points and minimum energy paths. J. Chem. Phys. **113**, 9901–9904 (2000)
23. Hu, S., Chen, L.: A phase-field model for evolving microstructures with strong elastic inhomogeneity. Acta Mater. **49**, 1879–1890 (2001)
24. Ionova, I., Carter, E.: Ridge method for finding saddle points on potential energy surfaces. J. Chem. Phys. **98**, 6377–6386 (1993)
25. Jerrad, R., Sternberg, P.: Critical points via Γ-convergence: general theory and applications. Preprint (2007)
26. Khachaturyan, A.: Theory of Structural Transformations in Solids. Wiley, New York (1983)
27. Kohn, R., Reznikoff, M., Tonegawa, Y.: The sharp-interface limit of the action functional for Allen-Cahn in one space dimension. Calc. Var. Partial Differ. Equ. **25**, 503–534 (2006)

28. Leo, P., Lowengrub, J., Jou, H.: A diffuse interface model for microstructure evolution in elastically stressed solids. Acta Mater. **61**, 2113–2130 (1998)
29. Li, X., Thornton, K., Nie, Q., Voorhees, P., Lowengrub, J.: Two- and three-dimensional equilibrium morphology of a misfitting particle and the Gibbs-Thomson effect. Acta Mater. **52**, 5829–5843 (2004)
30. Li, Y., Zhou, J.: A minimax method for finding multiple critical points and its applications to semilinear PDE. SIAM J. Sci. Comput. **23**, 840–865 (2001)
31. Moré, J., Munson, T.: Computing mountain passes and transition states. Math. Program. **100**, 151–182 (2004)
32. Onuki, A.: Ginzburg-Landau approach to elastic effects in the phase-separation of solids. J. Phys. Soc. Jpn. **58**, 3065–3068 (1989)
33. Poduri, R., Chen, L.: Non-classical nucleation theory of ordered intermetallic precipitates—application to the Al-Li alloy. Acta Mater. **44**, 4253–4259 (1996)
34. Rabinowitz, P.: Minimax Methods in Critical Point Theory with Applications to Differential Equations. Am. Math. Soc., Providence (1986)
35. Roy, A., Rickman, J., Gunton, J., Elder, K.: Simulation study of nucleation in a phase-field model with nonlocal interactions. Phys. Rev. E **57**, 2610–2617 (1998)
36. Sagui, C., Somoza, A.M., Desai, R.: Spinodal decomposition in an order-disorder phase-transition with elastic fields. Phys. Rev. E **50**, 4865–4879 (1994)
37. Wang, Y., Chen, L.Q., Khachaturyan, A.G.: Kinetics of strain-induced morphological transformation in cubic alloys with a miscibility gap. Acta Mater. **41**, 279–296 (1993)
38. Wang, Y., Khachaturyan, A.: Three-dimensional field model and computer modeling of martensitic transformations. Acta Mater. **45**, 759–773 (1997)
39. Yu, P., Hu, S., Du, Q., Chen, L.: An iterative-perturbation scheme for treating inhomogeneous elasticity in phase-field models. J. Comput. Phys. **208**, 34–50 (2005)
40. Zhang, L., Chen, L., Du, Q.: Morphology of critical nuclei in solid state phase transformations. Phys. Rev. Lett. **98**, 265703 (2007)
41. Zhang, L., Chen, L., Du, Q.: Diffuse-interface description of strain-dominated morphology of critical nuclei in phase transformations. Acta Mater. (2008). doi:10.1016/j.actamat.2008.03.043